压电/压磁复合楔形结构耦合场的奇异性研究:反平面问题*

王国林[1,2], 温建俊[2], 岳彦美[3], 刘金喜[1,3]

(1. 石家庄铁道大学 省部共建交通工程结构力学行为与系统安全国家重点实验室, 石家庄 050043;
2. 石家庄铁道大学 土木工程学院, 石家庄 050043;
3. 石家庄铁道大学 工程力学系, 石家庄 050043)

摘要: 研究了反平面变形状态下压电/压磁复合楔形结构耦合场的奇异性.应用复变函数理论和本征函数展开方法,推导了 16 种机械、电学和磁学组合边界条件下关于奇异性指数本征方程的显函表达式.基于得到的本征方程,通过数值算例表明了楔角、边界条件和材料组合类型对耦合场奇异性的影响,发现压电效应和压磁效应之间的相互作用导致压电/压磁复合楔磁电弹场的奇异性比压电复合楔电弹场的奇异性更加复杂.

关 键 词: 压电材料; 压磁材料; 复合楔形结构; 反平面变形; 耦合场; 奇异性指数
中图分类号: O343　　**文献标志码:** A　　DOI: 10.21656/1000-0887.450244

Singularities of Coupled Fields in Piezoelectric/Piezomagnetic Composite Wedges: an Antiplane Problem

WANG Guolin[1,2], WEN Jianjun[2], YUE Yanmei[3], LIU Jinxi[1,3]

(1. *State Key Laboratory of Mechanical Behavior and System Safety of Traffic Engineering Structures, Shijiazhuang Tiedao University, Shijiazhuang* 050043, *P.R.China*;
2. *School of Civil Engineering, Shijiazhuang Tiedao University, Shijiazhuang* 050043, *P.R.China*;
3. *Department of Engineering Mechanics, Shijiazhuang Tiedao University, Shijiazhuang* 050043, *P.R.China*)

Abstract: The singularities of the coupled fields near the apex of a piezoelectric/piezomagnetic composite wedge under antiplane deformation were studied. With the complex variable function theory and the eigenfunction expansion method, the explicit expressions of the eigenfunction equations for singularity orders were derived for 16 combinations of mechanically free or clamped, electrically closed or open and magnetically closed or open ones. Based on the obtained eigenequations, some numerical results were given to show the influences of the wedge angles, boundary conditions and material combination types on the singular behaviors. The results show that, the singularities of the coupled fields in a piezoelectric/piezomagnetic composite wedge are more

* **收稿日期:** 2024-09-06; **修订日期:** 2024-09-25
基金项目: 国家自然科学基金(11272222);河北省高等学校科学技术研究项目(QN2020204)
作者简介: 王国林(1990—),男,实验师,博士(E-mail: wangglstdu@163.com);
刘金喜(1961—),男,教授,博士,博士生导师(通讯作者. E-mail: liujx02@hotmail.com).
引用格式: 王国林, 温建俊, 岳彦美, 刘金喜. 压电/压磁复合楔形结构耦合场的奇异性研究:反平面问题[J]. 应用数学和力学, 2024, **45**(10): 1256-1267.

complicated than those in a piezoelectric counterpart.

Key words: piezoelectric material; piezomagnetic material; composite wedge; anti-plane deformation; coupled field; singularity order

0　引　　言

由压电材料和压磁材料制作而成的复合材料或结构可以实现电能和磁能之间的相互转换,即宏观上具有磁电耦合效应.压电/压磁复合材料除具有独特的磁电耦合外,仍具有力电和力磁耦合效应,因此,这类材料也称为磁电复合材料或磁电弹材料.按照复合方式和几何构型,压电/压磁复合材料一般可分为颗粒、纤维和层状三种形式[1].与颗粒和纤维两种形式的磁电复合材料相比,层状磁电复合材料不仅制备工艺简单,更重要的是磁电转换效率高,且易于施加电场或磁场来实现磁电性能的调控,同时也是众多磁电器件的主要结构形式.因此,除凝聚态物理和材料领域的研究人员们围绕层状磁电复合材料的磁电性能和器件应用开展了大量的工作外[1-7],力学工作者们从力-电-磁多场耦合的角度,重点研究了其振动[8-12]和弹性波传播[13-18]的动态特性以及界面断裂行为[19-25].

磁电效应是借助于界面传递变形而产生的,因此界面的结合强度对磁电转换以及磁电器件的可靠性有举足轻重的影响.对于层状磁电复合材料或器件,不可避免地会存在几何或材料性能的不连续区域,如图 1 所示.类似于孔洞、裂纹或位错等缺陷,楔形复合结构中几何形状的突变或材料性能的间断会导致楔顶(切口)附近产生应力集中,在线弹性理论范畴内,会出现应力趋于无穷大的现象,即具有应力奇异性[26-28].当压电、压磁和磁电效应存在时,不仅出现应力奇异性,电场和磁场也会出现奇异性,这将引起楔顶附近界面开裂、退极化或退磁化,进而导致磁电复合材料或器件破坏或丧失所希望的功能.因此,研究磁电复合楔形结构耦合场的奇异性对于进一步分析磁电复合材料或结构的断裂行为和失效机理非常重要.

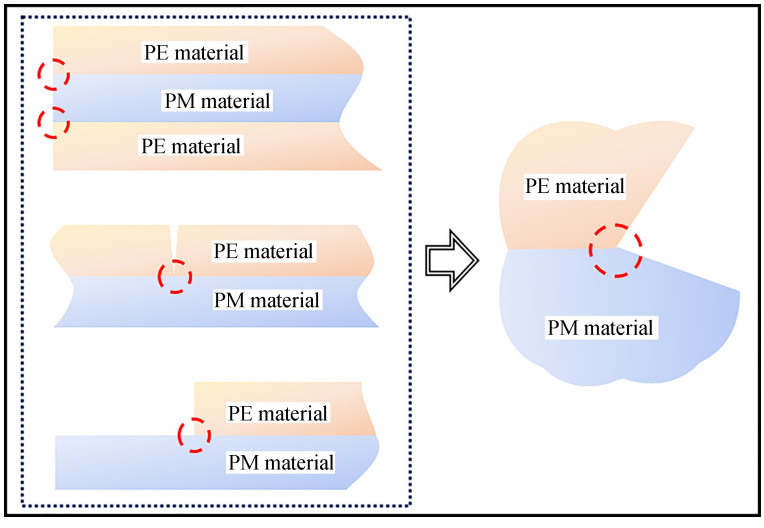

图 1　层状磁电复合材料及楔形结构模型

Fig. 1　Layered magnetoelectric composites and the wedge model

基于磁电弹全耦合理论,Liu 和 Chue[29]最先研究了反平面变形下横观各向同性磁电弹双材料楔形结构耦合场的奇异性;考虑机械自由-电学开路-磁学短路和机械固支-电学短路-磁学开路构成的三种边界条件,应用 Mellin 变换得到了显函形式的本征方程,分析本征方程发现,当两种材料的楔角相等以及边界条件关于界面对称时,奇异性与材料性能无关;他们以 $BaTiO_3$(BTO)/$CoFe_2O_4$(CFO)颗粒复合材料为例(BTO 为夹杂,CFO 为基体)分析了几种双材料楔的奇异性,包括磁电弹单材料楔、磁电弹双材料楔以及磁电弹材料分别与压电(PZT-4)、压磁(Terfenol-D)和 Glass-epoxy 组成的双材料,数值表明了楔角和材料组合形式对奇异性的影响.使用本征函数展开方法,Sue 等[30]也研究了同样的问题,给出了奇异性指数为实根时楔角和材料性能应该满足的条件.考虑到磁电弹双材料楔形结构中切口区域空气的存在,Liu[31]详细分析了磁电弹双材

料楔的奇异性,发现当材料的介电常数和磁导率接近空气的介电常数和磁导率时,磁电弹场的奇异性程度显著降低.对于边界上机械自由、电学开路和磁学短路的磁电弹多材料楔形结构,Zhou 等[32]应用辛方法研究了楔角和材料组合类型对磁电弹场奇异性的影响,给出了楔顶附近区域应力、电位移、磁感应强度和电场的分布特征.基于渐进展开法,程长征等[33]将求解偏微分方程组的边值问题转化为在给定边界条件下求解常微分方程组的线性本征值问题,然后利用插值矩阵法得到了单一磁电材料和双磁电弹材料楔的奇异性指数.使用同样的方法,Yang 等[34]研究了功能梯度磁电弹材料楔磁电弹场的奇异性问题,数值显示了功能梯度参数对奇异性指数的影响.

上述楔形结构中使用的磁电弹材料均是由 BTO 颗粒和 CFO 基体制作而成的复合材料.基于图 1 所示层状磁电复合材料的结构形式和特点,本文研究了压电/压磁双材料楔形结构耦合场的奇异性,主要目的是揭示楔角、边界条件、材料组合类型以及力电和力磁耦合之间相互作用对奇异性特征的影响规律.

1 问 题 描 述

本文考虑的磁电复合楔形结构如图 2 所示.它由楔角分别为 α 和 β 的压电楔和压磁楔完好黏结而成,压电楔和压磁楔均具有横观各向同性性能,x_1Ox_2 平面为两种材料的各向同性面,极化和磁化方向垂直于各向同性面.

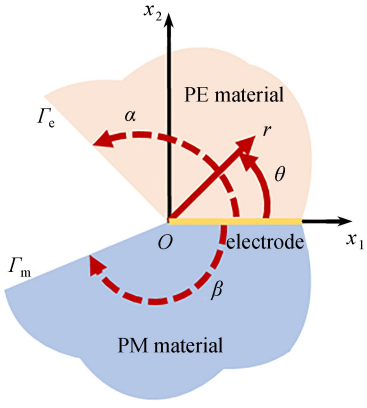

图 2 压电/压磁复合楔形结构

Fig. 2 A piezoelectric (PE)/ piezomagnetic (PM) composite wedge

对于反平面压电耦合问题,压电材料的面外位移和面内的电场是相互耦合的,在极坐标系下,本构方程和平衡方程如下[35]:

$$\begin{cases} \sigma_{3r}^{e} = c_{44}^{e}\dfrac{\partial u_3^{e}}{\partial r} + e_{15}\dfrac{\partial \varphi}{\partial r},\ \sigma_{3\theta}^{e} = \dfrac{1}{r}\left(c_{44}^{e}\dfrac{\partial u_3^{e}}{\partial \theta} + e_{15}\dfrac{\partial \varphi}{\partial \theta}\right), \\ D_r = e_{15}\dfrac{\partial u_3^{e}}{\partial r} - \varepsilon_{11}\dfrac{\partial \varphi}{\partial r},\ D_\theta = \dfrac{1}{r}\left(e_{15}\dfrac{\partial u_3^{e}}{\partial \theta} - \varepsilon_{11}\dfrac{\partial \varphi}{\partial \theta}\right), \end{cases} \tag{1}$$

$$\begin{cases} \dfrac{\partial}{\partial r}(r\sigma_{3r}^{e}) + \dfrac{\partial}{\partial \theta}\sigma_{3\theta}^{e} = 0, \\ \dfrac{\partial}{\partial r}(rD_r) + \dfrac{\partial}{\partial \theta}D_\theta = 0, \end{cases} \tag{2}$$

式中,u_3^{e} 和 φ 分别为位移和电势,σ_{3j}^{e} 和 $D_j(j=r,\ \theta)$ 分别为应力和电位移;c_{44}^{e},e_{15} 和 ε_{11} 分别为弹性、压电和介电常数;上标“e”表示与压电材料相应的量.将方程(1)代入方程(2),得到反平面压电问题的控制微分方程如下:

$$\begin{cases} c_{44}^{e}\nabla^2 u_3^{e} + e_{15}\nabla^2\varphi = 0, \\ e_{15}\nabla^2 u_3^{e} - \varepsilon_{11}\nabla^2\varphi = 0, \end{cases} \tag{3}$$

其中,$\nabla^2 = \partial^2/\partial r^2 + (1/r)\partial/\partial r + (1/r^2)\partial^2/\partial\theta^2$ 为极坐标下的 Laplace 算子.

类似于压电材料,压磁材料反平面力磁耦合的本构方程和平衡方程为

$$\begin{cases}\sigma_{3r}^{\mathrm{m}}=c_{44}^{\mathrm{m}}\dfrac{\partial u_3^{\mathrm{m}}}{\partial r}+h_{15}\dfrac{\partial \psi}{\partial r},\ \sigma_{3\theta}^{\mathrm{m}}=\dfrac{1}{r}\left(c_{44}^{\mathrm{m}}\dfrac{\partial u_3^{\mathrm{m}}}{\partial \theta}+h_{15}\dfrac{\partial \psi}{\partial \theta}\right),\\ B_r=h_{15}\dfrac{\partial u_3^{\mathrm{m}}}{\partial r}-\mu_{11}\dfrac{\partial \psi}{\partial r},\ B_\theta=\dfrac{1}{r}\left(h_{15}\dfrac{\partial u_3^{\mathrm{m}}}{\partial \theta}-\mu_{11}\dfrac{\partial \psi}{\partial \theta}\right),\end{cases} \tag{4}$$

$$\begin{cases}\dfrac{\partial}{\partial r}(r\sigma_{3r}^{\mathrm{m}})+\dfrac{\partial}{\partial \theta}\sigma_{3\theta}^{\mathrm{m}}=0,\\ \dfrac{\partial}{\partial r}(rB_r)+\dfrac{\partial}{\partial \theta}B_\theta=0,\end{cases} \tag{5}$$

其中,ψ 表示磁势,$B_j(j=r,\ \theta)$ 为磁感应强度;h_{15} 和 μ_{11} 分别为压磁常数和磁导率;上标“m”表示与压磁材料相应的量.将方程(4)代入方程(5),得到反平面压磁问题的控制微分方程为

$$\begin{cases}c_{44}^{\mathrm{m}}\nabla^2 u_3^{\mathrm{m}}+h_{15}\nabla^2\psi=0,\\ h_{15}\nabla^2 u_3^{\mathrm{m}}-\mu_{11}\nabla^2\psi=0.\end{cases} \tag{6}$$

压电楔中的电场和压磁楔中的磁场可通过

$$E_r=-\frac{\partial \varphi}{\partial r},\ E_\theta=-\frac{\partial \varphi}{r\partial \theta},\ H_r=-\frac{\partial \psi}{\partial r},\ E_\theta=-\frac{\partial \psi}{r\partial \theta} \tag{7}$$

得到.

在压电材料的边界 Γ_{e} 上,机械条件可以是机械自由或固支的,电学边界条件包括电学开路或短路两种情况,式(8)—(11)给出了可能的 4 种电弹边界条件:

FE(mechanically free-electrically closed):

$$\sigma_{3\theta}^{\mathrm{e}}(r,\alpha)=0,\ E_r(r,\alpha)=0; \tag{8}$$

FD(mechanically free-electrically open):

$$\sigma_{3\theta}^{\mathrm{e}}(r,\alpha)=0,\ D_\theta(r,\alpha)=0; \tag{9}$$

CE(mechanically clamped-electrically closed):

$$u_3^{\mathrm{e}}(r,\alpha)=0,\ E_r(r,\alpha)=0; \tag{10}$$

CD(mechanically clamped-electrically open):

$$u_3^{\mathrm{e}}(r,\alpha)=0,\ D_\theta(r,\alpha)=0. \tag{11}$$

根据电磁学理论和文献[36],当压磁材料边界 Γ_{m} 上的磁势为零(切向磁场为零)或法向磁感应强度为零时,分别称为磁学开路或磁学短路,这不同于压电材料;磁学短路可通过在结构表面覆盖金属或超导薄层来实现,磁学开路可通过在结构表面覆盖磁导率远大于 1 的薄层磁介质来实现.压磁楔边界上可能的磁弹边界条件如下:

FH(mechanically free-magnetically open):

$$\sigma_{3\theta}^{\mathrm{m}}(r,\ -\beta)=0,\ H_r(r,\ -\beta)=0; \tag{12}$$

FB(mechanically free-magnetically closed):

$$\sigma_{3\theta}^{\mathrm{m}}(r,\ -\beta)=0,\ B_\theta(r,\ -\beta)=0; \tag{13}$$

CH(mechanically clamped-magnetically open):

$$u_3^{\mathrm{m}}(r,\ -\beta)=0,\ H_r(r,\ -\beta)=0; \tag{14}$$

CB(mechanically clamped-magnetically closed):

$$u_3^{\mathrm{m}}(r,\ -\beta)=0,\ B_\theta(r,\ -\beta)=0. \tag{15}$$

对于所考虑的压电/压磁楔形体,共有 16 种形式的组合边界条件,在第 2 节中将详细列出各边界条件及其本征方程的显函表达式.

为了施加电场或输出电信号,磁电层状复合材料中的压电层和压磁层通常用非常薄的导电银胶黏结[37-41],基于这一物理背景,本文将界面视为不考虑厚度的电极.因此,压电和压磁之间的界面条件为

$$\begin{cases} u_3^{\mathrm{e}}(r,0) = u_3^{\mathrm{m}}(r,0),\ \sigma_{3\theta}^{\mathrm{e}}(r,0) = \sigma_{3\theta}^{\mathrm{m}}(r,0), \\ E_r(r,0) = 0,\ B_\theta(r,0) = 0. \end{cases} \tag{16}$$

2 问题的解及本征方程

首先推导压电楔中电弹场的解.根据复变函数理论,方程(3)的位移和电势可以用两个解析函数 $U_3^{\mathrm{e}}(z)$ 和 $\boldsymbol{\Phi}(z)$ 表示为

$$u_3^{\mathrm{e}} = \mathrm{Re}[U_3^{\mathrm{e}}(z)],\ \varphi = \mathrm{Re}[\boldsymbol{\Phi}(z)], \tag{17}$$

式中,"Re"表示取实部,$z = r\mathrm{e}^{\mathrm{i}\theta}$,$\mathrm{i} = \sqrt{-1}$.

基于本征函数展开方法,楔形结构反平面压电问题的解可设为

$$\begin{cases} U_3^{\mathrm{e}} = a_1 r^{\lambda}\mathrm{e}^{\mathrm{i}\lambda\theta} + a_2 r^{\bar{\lambda}}\mathrm{e}^{\mathrm{i}\bar{\lambda}\theta}, \\ \boldsymbol{\Phi} = a_3 r^{\lambda}\mathrm{e}^{\mathrm{i}\lambda\theta} + a_4 r^{\bar{\lambda}}\mathrm{e}^{\mathrm{i}\bar{\lambda}\theta}, \end{cases} \tag{18}$$

其中 $a_i(i = 1,2,3,4)$ 是未知的常数,λ 为本征值,$\bar{\lambda}$ 是 λ 的共轭.将式(18)代入式(17),可得到

$$\begin{cases} u_3^{\mathrm{e}} = \mathrm{Re}\{r^{\lambda}[c_1\cos(\lambda\theta) + c_2\sin(\lambda\theta)]\}, \\ \varphi = \mathrm{Re}\{r^{\lambda}[c_3\cos(\lambda\theta) + c_4\sin(\lambda\theta)]\}, \end{cases} \tag{19}$$

其中,$c_1 = a_1 + \bar{a}_2$,$c_2 = \mathrm{i}(a_1 - \bar{a}_2)$,$c_3 = a_3 + \bar{a}_4$,$c_4 = \mathrm{i}(a_3 - \bar{a}_4)$.使用上式和本构关系(1),得到应力、电位移和电场如下:

$$\begin{cases} \sigma_{3r}^{\mathrm{e}} = \mathrm{Re}\{\lambda r^{\lambda-1}[c_{44}^{\mathrm{e}}(c_1\cos(\lambda\theta) + c_2\sin(\lambda\theta)) + e_{15}(c_3\cos(\lambda\theta) + c_4\sin(\lambda\theta))]\}, \\ \sigma_{3\theta}^{\mathrm{e}} = \mathrm{Re}\{\lambda r^{\lambda-1}[c_{44}^{\mathrm{e}}(c_2\cos(\lambda\theta) - c_1\sin(\lambda\theta)) - e_{15}(c_3\sin(\lambda\theta) - c_4\cos(\lambda\theta))]\}, \end{cases} \tag{20}$$

$$\begin{cases} D_r = \mathrm{Re}\{\lambda r^{\lambda-1}[e_{15}(c_1\cos(\lambda\theta) + c_2\sin(\lambda\theta)) - \varepsilon_{11}(c_3\cos(\lambda\theta) + c_4\sin(\lambda\theta))]\}, \\ D_\theta = \mathrm{Re}\{\lambda r^{\lambda-1}[e_{15}(c_2\cos(\lambda\theta) - c_1\sin(\lambda\theta)) + \varepsilon_{11}(c_3\sin(\lambda\theta) - c_4\cos(\lambda\theta))]\}, \end{cases} \tag{21}$$

$$\begin{cases} E_r = -\partial\varphi/\partial r = -\mathrm{Re}\{\lambda r^{\lambda-1}[c_3\cos(\lambda\theta) + c_4\sin(\lambda\theta)]\}, \\ E_\theta = -\partial\varphi/(r\partial\theta) = -\mathrm{Re}\{\lambda r^{\lambda-1}[c_4\cos(\lambda\theta) - c_3\sin(\lambda\theta)]\}. \end{cases} \tag{22}$$

与压电材料类似,压磁楔的位移及磁势为

$$\begin{cases} u_3^{\mathrm{m}} = \mathrm{Re}\{r^{\lambda}[c_5\cos(\lambda\theta) + c_6\sin(\lambda\theta)]\}, \\ \psi = \mathrm{Re}\{r^{\lambda}[c_7\cos(\lambda\theta) + c_8\sin(\lambda\theta)]\}. \end{cases} \tag{23}$$

将其代入压磁材料的本构方程(4),得到应力、磁感应强度及磁场强度如下:

$$\begin{cases} \sigma_{3r}^{\mathrm{m}} = \mathrm{Re}\{\lambda r^{\lambda-1}[c_{44}^{\mathrm{m}}(c_5\cos(\lambda\theta) + c_6\sin(\lambda\theta)) + h_{15}(c_7\cos(\lambda\theta) + c_8\sin(\lambda\theta))]\}, \\ \sigma_{3\theta}^{\mathrm{m}} = \mathrm{Re}\{\lambda r^{\lambda-1}[c_{44}^{\mathrm{m}}(c_6\cos(\lambda\theta) - c_5\sin(\lambda\theta)) - h_{15}(c_7\sin(\lambda\theta) - c_8\cos(\lambda\theta))]\}, \end{cases} \tag{24}$$

$$\begin{cases} B_r = \mathrm{Re}\{\lambda r^{\lambda-1}[h_{15}(c_5\cos(\lambda\theta) + c_6\sin(\lambda\theta)) - \mu_{11}(c_7\cos(\lambda\theta) + c_8\sin(\lambda\theta))]\}, \\ B_\theta = \mathrm{Re}\{\lambda r^{\lambda-1}[h_{15}(c_6\cos(\lambda\theta) - c_5\sin(\lambda\theta)) + \mu_{11}(c_7\sin(\lambda\theta) - c_8\cos(\lambda\theta))]\}, \end{cases} \tag{25}$$

$$\begin{cases} H_r = -\partial\psi/\partial r = -\mathrm{Re}\{\lambda r^{\lambda-1}[c_7\cos(\lambda\theta) + c_8\sin(\lambda\theta)]\}, \\ H_\theta = -\partial\varphi/(r\partial\theta) = -\mathrm{Re}\{\lambda r^{\lambda-1}[c_8\cos(\lambda\theta) - c_7\sin(\lambda\theta)]\}. \end{cases} \tag{26}$$

基于以上各个场量的解,可以得到每一组边界条件下关于奇异性指数的本征方程.下面以 Γ_{e} 和 Γ_{m} 两个边界上机械自由、电学开路和磁学短路组成的边界条件推导本征方程.

对于压电边界上为机械自由-电学开路(FD)的情况,可得到

$$\begin{cases} c_{44}^{\mathrm{e}}[c_2\cos(\lambda\alpha) - c_1\sin(\lambda\alpha)] - e_{15}[c_3\sin(\lambda\alpha) + c_4\cos(\lambda\alpha)] = 0, \\ e_{15}[c_2\cos(\lambda\alpha) - c_1\sin(\lambda\alpha)] + \varepsilon_{11}[c_3\sin(\lambda\alpha) - c_4\cos(\lambda\alpha)] = 0. \end{cases} \tag{27}$$

当压磁边界为机械自由-磁学短路(FB)时,有

$$\begin{cases} c_{44}^{\mathrm{m}}[c_6\cos(\lambda\beta) + c_5\sin(\lambda\beta)] + h_{15}[c_7\sin(\lambda\beta) + c_8\cos(\lambda\beta)] = 0, \\ h_{15}[c_6\cos(\lambda\beta) + c_5\sin(\lambda\beta)] - \mu_{11}[c_7\sin(\lambda\beta) + c_8\cos(\lambda\beta)] = 0. \end{cases} \tag{28}$$

利用式(16)中的界面条件,可得

$$c_1 = c_5,\ c_{44}^{e}c_2 - e_{15}c_4 = c_{44}^{m}c_6 + h_{15}c_8,\ c_3 = 0,\ h_{15}c_6 - \mu_{11}c_8 = 0. \tag{29}$$

方程(27)—(29)为关于 $c_i(i = 1,2,\cdots,8)$ 的齐次线性方程组,其非零解要求其系数矩阵的行列式必须为零.求解并化简后得到压电/压磁楔形结构在 FD/FB 边界条件下的本征方程为

$$\cos(\lambda\alpha)[c_{44}^{e}\sin(\lambda\alpha)\cos(\lambda\beta) + \bar{c}_{44}^{m}\cos(\lambda\alpha)\sin(\lambda\beta)] = 0. \tag{30}$$

应用同样的分析过程,可以得到其他 15 种组合边界条件下本征方程的显函表达式.16 种组合边界条件本征方程的显函表达式如式(31)—(46)所示:

FD/FB:

$$\cos(\lambda\alpha)[c_{44}^{e}\sin(\lambda\alpha)\cos(\lambda\beta) + \bar{c}_{44}^{m}\cos(\lambda\alpha)\sin(\lambda\beta)] = 0; \tag{31}$$

FD/FH:

$$\cos(\lambda\alpha)[(c_{44}^{m}/c_{44}^{e})\cos(\lambda\alpha)\sin(2\lambda\beta)/2 + \sin(\lambda\alpha)\cos^2(\lambda\beta) + k_m^2\sin(\lambda\alpha)\sin^2(\lambda\beta)] = 0; \tag{32}$$

FE/FB:

$$\sin(\lambda\alpha)[c_{44}^{e}\sin(\lambda\alpha)\cos(\lambda\beta) + \bar{c}_{44}^{m}\cos(\lambda\alpha)\sin(\lambda\beta)] = 0; \tag{33}$$

FE/FH:

$$\sin(\lambda\alpha)[(c_{44}^{m}/c_{44}^{e})\cos(\lambda\alpha)\sin(2\lambda\beta)/2 + \sin(\lambda\alpha)\cos^2(\lambda\beta) + k_m^2\sin(\lambda\alpha)\sin^2(\lambda\beta)] = 0; \tag{34}$$

CD/CB:

$$(\bar{c}_{44}^{m}/\bar{c}_{44}^{e})\sin(2\lambda\alpha)\cos(\lambda\beta)/2 + \cos^2(\lambda\alpha)\sin(\lambda\beta) + k_e^2\sin^2(\lambda\alpha)\sin(\lambda\beta) = 0; \tag{35}$$

CD/CH:

$$(\bar{c}_{44}^{m}/\bar{c}_{44}^{e})\sin(2\lambda\alpha)\cos(\lambda\beta)/2 + \cos^2(\lambda\alpha)\sin(\lambda\beta) + k_e^2\sin^2(\lambda\alpha)\sin(\lambda\beta) = 0; \tag{36}$$

CE/CB:

$$\sin(\lambda\alpha)[c_{44}^{e}\cos(\lambda\alpha)\sin(\lambda\beta) + \bar{c}_{44}^{m}\sin(\lambda\alpha)\cos(\lambda\beta)] = 0; \tag{37}$$

CE/CH:

$$c_{44}^{e}\cos(\lambda\alpha)\sin(\lambda\beta) + \bar{c}_{44}^{m}\sin(\lambda\alpha)\cos(\lambda\beta) = 0; \tag{38}$$

FD/CB:

$$\cos(\lambda\alpha)[c_{44}^{e}\sin(\lambda\alpha)\sin(\lambda\beta) - \bar{c}_{44}^{m}\cos(\lambda\alpha)\cos(\lambda\beta)] = 0; \tag{39}$$

FD/CH:

$$\cos(\lambda\alpha)[c_{44}^{e}\sin(\lambda\alpha)\sin(\lambda\beta) - \bar{c}_{44}^{m}\cos(\lambda\alpha)\cos(\lambda\beta)] = 0; \tag{40}$$

FE/CB:

$$\sin(\lambda\alpha)[c_{44}^{e}\sin(\lambda\alpha)\sin(\lambda\beta) - \bar{c}_{44}^{m}\cos(\lambda\alpha)\cos(\lambda\beta)] = 0; \tag{41}$$

FE/CH:

$$\cos(\lambda\beta)[c_{44}^{e}\sin(\lambda\alpha)\sin(\lambda\beta) - \bar{c}_{44}^{m}\cos(\lambda\alpha)\cos(\lambda\beta)] = 0; \tag{42}$$

CD/FB:

$$\cos^2(\lambda\alpha)\cos(\lambda\beta) + k_e^2\sin^2(\lambda\alpha)\cos(\lambda\beta) - (\bar{c}_{44}^{m}/\bar{c}_{44}^{e})\sin(2\lambda\alpha)\sin(\lambda\beta)/2 = 0; \tag{43}$$

CD/FH:

$$[k_m^2\sin^2(\lambda\beta) + \cos^2(\lambda\beta)][\cos^2(\lambda\alpha) + k_e^2\sin^2(\lambda\alpha)] - (c_{44}^{m}/\bar{c}_{44}^{e})\sin(2\lambda\alpha)\sin(2\lambda\beta)/4 = 0; \tag{44}$$

CE/FB:

$$\sin(\lambda\alpha)[c_{44}^{e}\cos(\lambda\alpha)\cos(\lambda\beta) - \bar{c}_{44}^{m}\sin(\lambda\alpha)\sin(\lambda\beta)] = 0; \tag{45}$$

CE/FH:

$$(c_{44}^{m}/c_{44}^{e})\sin(\lambda\alpha)\sin(2\lambda\beta)/2 - \cos(\lambda\alpha)\cos^2(\lambda\beta) - k_m^2\cos(\lambda\alpha)\sin^2(\lambda\beta) = 0, \tag{46}$$

式中,$\bar{c}_{44}^{e} = c_{44}^{e} + e_{15}^2/\varepsilon_{11}$ 和 $\bar{c}_{44}^{m} = c_{44}^{m} + h_{15}^2/\mu_{11}$ 分别为压电和压磁硬化的弹性刚度常数,$k_e = \sqrt{e_{15}^2/(\bar{c}_{44}^{e}\varepsilon_{11})}$ 和 $k_m = \sqrt{h_{15}^2/(\bar{c}_{44}^{m}\mu_{11})}$ 分别为压电和压磁耦合系数.

如果压磁材料的压磁系数 h_{15} 为零,那么压磁材料退化为导体,压电/压磁复合楔退化为压电/导体复合楔,其相应边界条件下的本征方程变为文献[42]得到的压电/导体复合楔的本征方程.对于所研究的问题,位

移、电势和磁势应该是有界的,当应力、电场和磁场在楔顶附近区域出现奇异性时,本征值 λ 应该满足

$$-1 < \mathrm{Re}(\lambda - 1) < 0. \tag{47}$$

3 数值算例及讨论

基于上一节得到的本征方程,本节将通过数值算例探究楔角、边界条件和材料组合类型对奇异性特征的影响.在算例中使用的压电材料为 BTO 和 PZT-4,压磁材料为 CFO 和 Terfenol-D(TFD),它们的材料常数在表 1 中给出.除特别说明外,压电楔的楔角 $\alpha = 180°$, 压磁楔的楔角 β 在 0°~180°之间变化.

表 1 材料常数

Table 1 Material constants

parameter	BTO[43]	PZT-4[44]	CFO[43]	TFD[45]
$c_{44}/(10^{10}\cdot\mathrm{N/m^2})$	4.3	2.56	4.53	0.599
$e_{15}/(\mathrm{C/m^2})$	11.6	12.7	–	–
$\varepsilon_{11}/(10^{-9}\cdot\mathrm{C^2/(N\cdot m^2)})$	11.2	6.46	–	–
$h_{15}/(\mathrm{N/(A\cdot m)})$	–	–	550	167.66
$\mu_{11}/(10^{-6}\cdot\mathrm{N\cdot S^2/C^2})$	–	–	590	3.98

图 3 和图 4 分别给出了机械自由、电学开路和磁学短路(FD/FB)以及机械自由、电学开路和磁学开路(FD/FH)边界条件下,BTO/CFO 和 PZT-4/CFO 两种复合楔耦合场奇异性指数的变化.由图 3 和图 4 可以看出,磁学短路条件下只存在一阶奇异性,但磁学开路条件下不仅存在二阶奇异性,而且还出现了振荡奇异性,振荡奇异性的范围分别为 $150°<\beta<180°$ 和 $159°<\beta<180°$;PZT-4/CFO 复合楔的一阶奇异性强于 BTO/CFO 复合楔的一阶奇异性; 当 $\beta\to180°$ 时, 即双材料楔的切口成为裂纹时, 磁学短路条件下, BTO/CFO 和 PZT-4/CFO 复合楔耦合场的奇异性为−0.5; 磁学开路条件下, BTO/CFO 和 PZT-4/CFO 复合楔耦合场的奇异性为−0.5±0.023 7i .

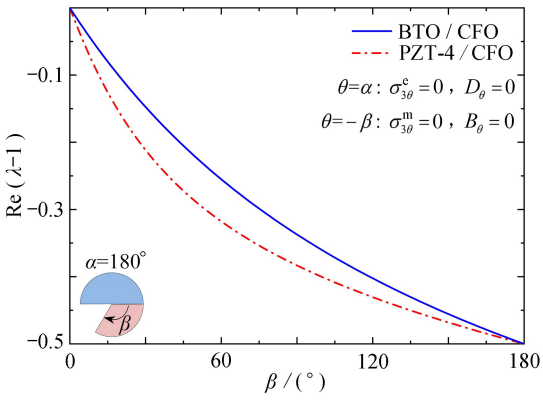

图 3 电学开路/磁学短路(FD/FB)边界下, BTO/CFO 和 PZT-4/CFO 楔的奇异性

Fig. 3 The singularity orders for BTO/CFO and PZT-4/CFO wedges with boundary condition combination FD/FB

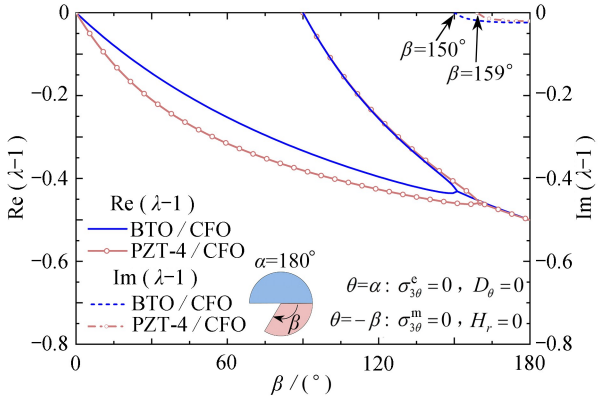

图 4 电学开路/磁学开路(FD/FH)边界下, BTO/CFO 和 PZT-4/CFO 楔的奇异性

Fig. 4 The singularity orders for BTO/CFO and PZT-4/CFO wedges with boundary condition combination FD/FH

注 为了解释图中的颜色,读者可以参考本文的电子网页版本,后同.

图 5 和图 6 表明了压磁材料性能差异对复合楔形结构耦合场奇异性的影响,这里压电材料为 BTO,压磁材料分别为 CFO 和 TFD .与图 3 和图 4 比较可以看到,压磁材料的不同并没有改变磁学短路和磁学开路条件下奇异性指数变化的基本特征;当压磁楔为 TFD 时,一阶奇异性从 $\beta > 0°$ 开始增强,超过某一角度后慢慢减弱,然后随着 β 的角度增大,奇异性强度增加,并与二阶奇异性的变化曲线重合;BTO/TFD 振荡奇异性程度不仅比 BTO/CFO 强,而且振荡奇异性存在的角度范围比 BTO/CFO 大.

从上面的结果可以发现,压电或压磁材料性能的不同只影响奇异性的强弱程度,而压磁楔边界上磁学边界条件的不同则改变了奇异性的基本特征.为揭示力学边界条件的影响,图 7 给出了机械固支-电学开路/机械自由-磁学开路(CD/FH)组合边界条件下,BTO/CFO 复合楔的奇异性变化.图 7 表明: 1) 奇异性的阶数达

到了 4 个; 2) 当$\beta\to0°$时,出现了-0.5 的奇异性, 这是因为压电/压磁复合楔成为压电半平面时,混合的力学和电学边界条件所引起的; 3) 一阶和二阶奇异性指数在$\beta=0°\sim127°$范围内是相等的,三阶和四阶奇异性指数则在$\beta=90°\sim104°$范围内是相等的,同时在这两个区间内存在振荡奇异性.

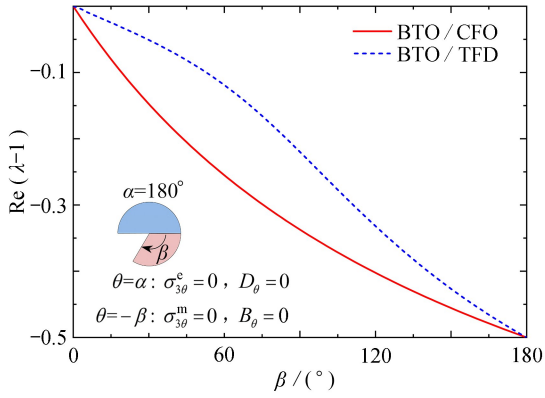

图 5　电学开路/磁学短路(FD/FB)边界下, BTO/CFO 和 BTO/TFD 楔的奇异性

Fig. 5　The singularity orders for BTO/CFO and BTO/TFD wedges with boundary condition combination FD/FB

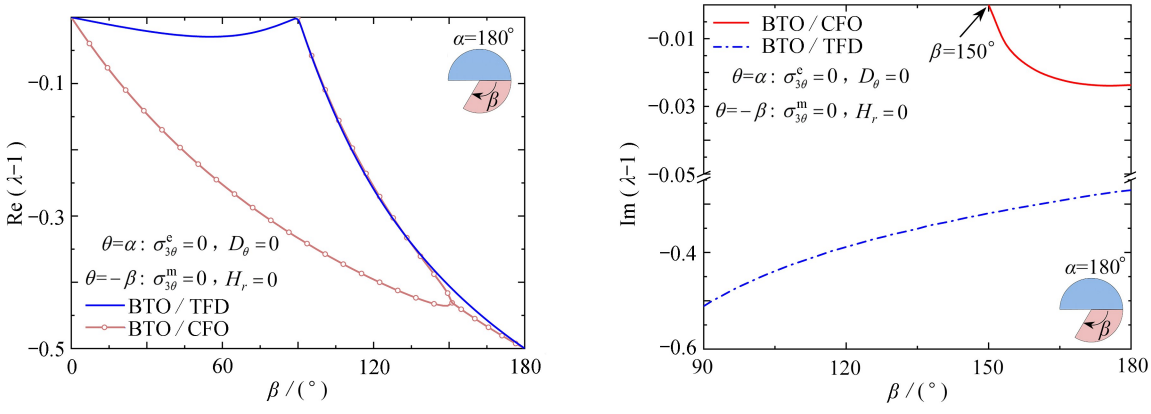

(a) 实部　　(b) 虚部

(a) Real part　　(b) Imaginary part

图 6　电学开路/磁学开路(FD/FH)边界下, BTO/CFO 和 BTO/TFD 楔的奇异性

Fig. 6　The singularity orders for BTO/CFO and BTO/TFD wedges with boundary condition combination FD/FH

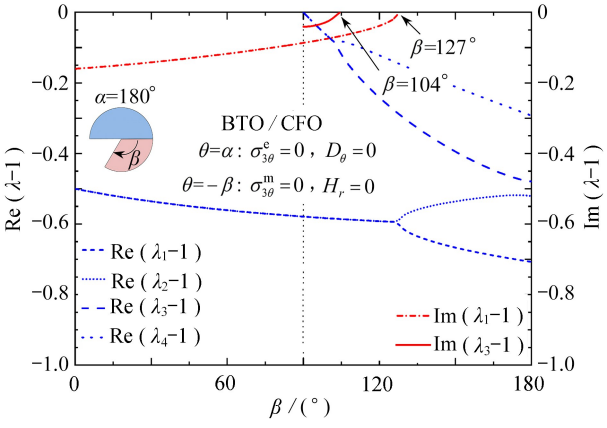

图 7　机械固支-电学开路和机械自由-磁学开路(CD/FH)边界下, BTO/CFO 楔的奇异性

Fig. 7　The singularity orders for the BTO/CFO wedge with boundary condition combination CD/FH

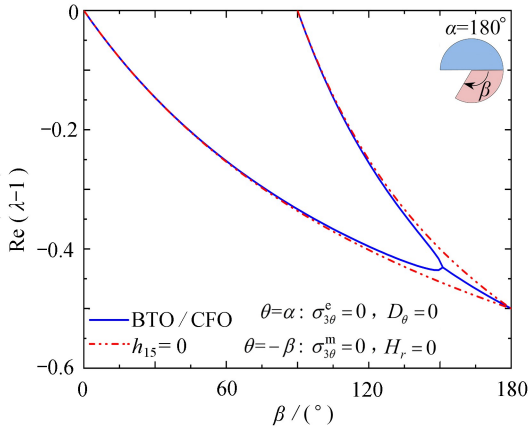

图 8　机械自由、电学开路和磁学开路(FD/FH)边界下, 力磁耦合对 BTO/CFO 楔奇异性的影响

Fig. 8　The effect of magnetomechanical coupling on the singularity orders of the BTO/CFO wedge under the FD/FH boundary

从式(31)—(46)所列 16 种边界下的本征方程可以观察到,只有压电楔边界上为机械固支-电学开路时,奇异性同时与压电效应和压磁效应有关.为了表明压磁效应的影响,图 8 表明了应力自由、电学开路/磁学开路(FD/FH)条件下忽略压磁效应时,BTO/CFO 的奇异性.从该图中可以看出,没有力磁耦合的情况下,不再出现振荡奇异性.

上面主要讨论了固定压电楔楔角时边界条件和材料组合类型对奇异性的影响规律.为了分析压电楔和压磁楔的楔角同时变化时的奇异性,图 9 和图 10 给出了机械自由、电学开路、磁学短路或开路两种边界条件下,PZT-4/CFO 复合楔最强奇异性的变化.图 9 表明,对于机械自由-电学开路/机械自由-磁学短路(FD/FB)边界条件,在 $\alpha+\beta=180°$附近区域开始出现奇异性,且奇异性指数都是实数.从图 10 中可以看到:1) 当压磁楔的边界磁学开路时,存在振荡奇异性,这与图 4 的结果是一致的;2) 当 $\alpha<\beta$ 时,奇异性指数基本上与 α 角度的变化无关;3) 在 $\alpha>\beta$ 的区域,奇异性强度随 α 的增大而增强,裂纹时出现略强于−0.5 的奇异性;4) 振荡奇异性仅仅出现在 $\beta_1=1.12\alpha+1.84°$ 与 $\beta_2=0.9\alpha-1.49°$ 两线之间的范围内,而且比较弱.

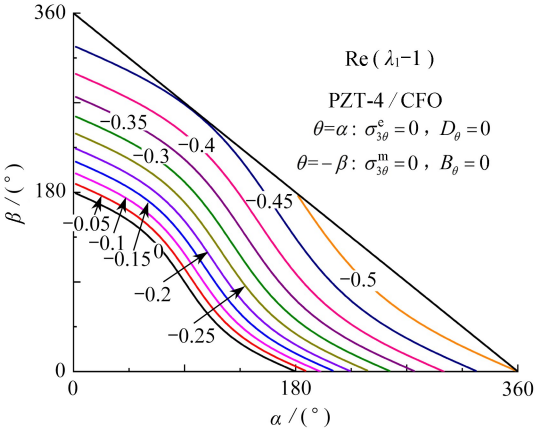

图 9 机械自由、电学开路和磁学短路(FD/FB)边界下, PZT-4/CFO 楔最强奇异性指数随楔角 α 和 β 的变化

Fig. 9 Variations of the strongest singularity orders of the PZT-4/CFO wedge under boundary condition combination FD/FB with wedge angles α and β

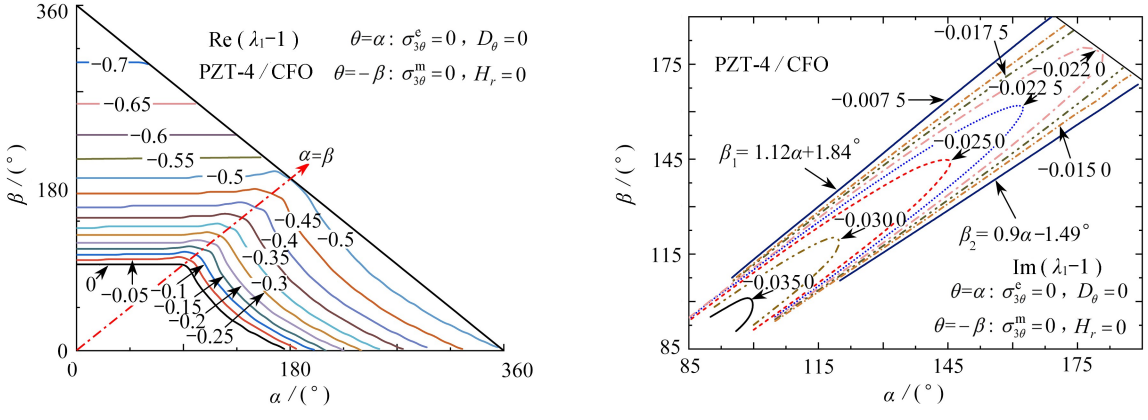

(a) 实部 (b) 虚部

(a) Real part (b) Imaginary part

图 10 机械自由、电学开路和磁学开路(FD/FH)边界下, PZT-4/CFO 楔最强奇异性指数随楔角 α 和 β 的变化

Fig. 10 Variations of the strongest singularity orders of the PZT-4/CFO wedge under the boundary condition combination FD/FH with wedge angles α and β

4 结 论

本文研究了反平面变形状态下压电/压磁双材料楔耦合场的奇异性,从边界条件的完备性考虑,推导了

16 种力、电、磁组合边界条件下奇异性指数的本征方程,通过数值算例重点分析了机械自由时磁学边界条件和材料差异对奇异性特征的影响.主要结论包括: 1) 磁学短路情况下,在 $\alpha+\beta=180°$ 附近开始出现奇异性,只存在一阶奇异性,且奇异性指数都是实数; 2) 与磁学短路相比,磁学开路情况下奇异性存在的楔角范围有所增大,最大区别是存在二阶奇异性和振荡奇异性; 3) 压电材料和压磁材料的组合形式以及力、电、磁组合边界条件的类型显著影响复合楔耦合场的奇异性特征.最后,应该指出的是,振荡奇异性的出现是因为材料性能和边界条件的差异导致特征方程的数学性质发生了变化.

参考文献(References):

[1] NAN C W, BICHURIN M I, DONG S X, et al. Multiferroic magnetoelectric composites: historical perspective, status, and future directions[J]. *Journal of Applied Physics*, 2008, **103**(3): 031101.

[2] ZHAI J Y, XING Z P, DONG S X, et al. Magnetoelectric laminate composites: an overview[J]. *Journal of the American Ceramic Society*, 2008, **91**(2): 351-358.

[3] SRINIVASAN G. Magnetoelectric composites[J]. *Annual Review of Materials Research*, 2010, **40**: 153-178.

[4] WANG Y J, LI J F, VIEHLAND D. Magnetoelectrics for magnetic sensor applications: status, challenges and perspectives[J]. *Materials Today*, 2014, **17**(6): 269-275.

[5] LEUNG C M, LI J F, VIEHLAND D, et al. A review on applications of magnetoelectric composites: from heterostructural uncooled magnetic sensors, energy harvesters to highly efficient power converters[J]. *Journal of Physics D: Applied Physics*, 2018, **51**(26): 263002.

[6] CHU Z Q, POURHOSSEINIASL M J, DONG S X. Review of multi-layered magnetoelectric composite materials and devices applications[J]. *Journal of Physics D: Applied Physics*, 2018, **51**(24): 243001.

[7] LIANG X F, MATYUSHOV A, HAYES P, et al. Roadmap on magnetoelectric materials and devices[J]. *IEEE Transactions on Magnetics*, 2021, **57**(8): 1-57.

[8] PAN E, HEYLIGER P R. Free vibrations of simply supported and multilayered magneto-electro-elastic plates [J]. *Journal of Sound and Vibration*, 2002, **252**(3): 429-442.

[9] BHANGALE R K, GANESAN N. Free vibration of simply supported functionally graded and layered magneto-electro-elastic plates by finite element method[J]. *Journal of Sound and Vibration*, 2006, **294**(4/5): 1016-1038.

[10] YANG Z X, DANG P F, HAN Q K, et al. Natural characteristics analysis of magneto-electro-elastic multilayered plate using analytical and finite element method[J]. *Composite Structures*, 2018, **185**: 411-420.

[11] NGAK F P E, NTAMACK G E, AZRAR L. Dynamic and static behaviors of multilayered angle-ply magnetoelectroelastic laminates with viscoelastic interfaces[J]. *Composite Structures*, 2018, **189**: 667-687.

[12] KUO H Y, WEI K H. Free vibration of multiferroic laminated composites with interface imperfections[J]. *Acta Mechanica*, 2022, **233**(9): 3699-3717.

[13] CHEN J Y, PAN E, CHEN H L. Wave propagation in magneto-electro-elastic multilayered plates[J]. *International Journal of Solids and Structures*, 2007, **44**(3/4): 1073-1085.

[14] 杜建科, 金小英, 王骥. 电磁弹性层状结构中的 Love 波传播[J]. 中国科学(G 辑): 物理学 力学 天文学, 2007, **37**(6): 789-803.(DU Jianke, JIN Xiaoying, WANG Ji. Love wave propagation in electromagnetic elastic layered structure[J]. *Science in China* (*Series G*): *Physics*, *Mechanics & Astronomy*, 2007, **37**(6): 789-803. (in Chinese))

[15] ZHOU Y Y, LÜ C F, CHEN W Q. Bulk wave propagation in layered piezomagnetic/piezoelectric plates with initial stresses or interface imperfections[J]. *Composite Structures*, 2012, **94**(9): 2736-2745.

[16] MATAR O B, GASMI N, ZHOU H, et al. Legendre and Laguerre polynomial approach for modeling of wave propagation in layered magneto-electro-elastic media[J]. *The Journal of the Acoustical Society of America*,

2013, **133**(3): 1415-1424.

[17] EZZIN H, AMOR M B, GHOZLEN M H B. Propagation behavior of SH waves in layered piezoelectric/piezomagnetic plates[J]. *Acta Mechanica*, 2017, **228**: 1071-1081.

[18] KUO H Y, WANG Y H. Wave motion of magneto-electro-elastic laminated plates with membrane-type interfacial imperfections[J]. *Composite Structures*, 2022, **293**: 115661.

[19] 张培伟, 周振功, 王彪. 不同功能梯度压电压磁层状介质中共线界面裂纹的动态性能分析[J]. 应用数学和力学, 2007, **28**(5): 551-560.(ZHANG Peiwei, ZHOU Zhengong, WANG Biao. Dynamic behavior of two collinear interface cracks between two dissimilar functionally graded piezoelectric/piezomagnetic material strips[J]. *Applied Mathematics and Mechanics*, 2007, **28**(5): 551-560.(in Chinese))

[20] WANG B L, HAN J C, DU S Y. Transient fracture of a layered magnetoelectroelastic medium[J]. *Mechanics of Materials*, 2010, **42**(3): 354-364.

[21] HERRMANN K P, LOBODA V V, KHODANEN T V. An interface crack with contact zones in a piezoelectric/piezomagnetic bimaterial[J]. *Archive of Applied Mechanics*, 2010, **80**: 651-670.

[22] WAN Y P, YUE Y P, ZHONG Z. Multilayered piezomagnetic/piezoelectric composite with periodic interface cracks under magnetic or electric field[J]. *Engineering Fracture Mechanics*, 2012, **84**: 132-145.

[23] GOVORUKHA V, KAMLAH M, LOBODA V, et al. Interface cracks in piezoelectric materials[J]. *Smart Materials and Structures*, 2016, **25**(2): 023001.

[24] 赵星. 压电-压磁夹层结构界面裂纹的断裂行为[D]. 南京: 南京航空航天大学, 2020.(ZHAO Xing. Fracture behavior of interface cracks in piezoelectric-piezomagnetic sandwich structure[D]. Nanjing: Nanjing University of Aeronautics and Astronautics, 2020.(in Chinese))

[25] 延真. 基于扩展有限单元法的压电-压磁双层结构界面裂纹断裂研究[D]. 石家庄: 石家庄铁道大学, 2021.(YAN Zhen. Fracture analysis of interfacial cracks in piezoelectric-piezomagnetic bi-layered structures by the extended finite element method[D]. Shijiazhuang: Shijiazhuang Tiedao University, 2021.(in Chinese))

[26] SAVRUK M P, KAZBERUK A. Stress concentration near sharp and rounded V-notches in orthotropic and quasi-orthotropic bodies[J]. *Theoretical and Applied Fracture Mechanics*, 2016, **84**: 166-176.

[27] PENADO F E. Analysis ofbimaterial singular regions for orthotropic and isotropic materials under thermal loading[J]. *Engineering Fracture Mechanics*, 2021, **243**: 107527.

[28] SHIN K C, KIM W S, LEE J J. Application of stress intensity to design of anisotropic/isotropic bi-materials with a wedge[J]. *International Journal of Solids and Structures*, 2007, **44**(24): 7748-7766.

[29] LIU T J C, CHUE C H. On the singularities in abimaterial magneto-electro-elastic composite wedge under anti-plane deformation[J]. *Composite Structures*, 2006, **72**(2): 254-265.

[30] SUE W C, LIOU J Y, SUNG J C. Investigation of the stress singularity of a magnetoelectroelastic bonded anti-plane wedge[J]. *Applied Mathematical Modelling*, 2007, **31**(10): 2313-2331.

[31] LIU T J C. The singularity problem of the magneto-electro-elastic wedge-junction structure with consideration of the air effect[J]. *Archive of Applied Mechanics*, 2009, **79**(5): 377-393.

[32] ZHOU Z H, XU X S, LEUNG A Y T. Hamiltonian analysis of a magnetoelectroelastic notch in a mode Ⅲ singularity[J]. *Smart Materials and Structures*, 2013, **22**(9): 095018.

[33] 程长征, 丁昊, 王大鹏, 等. 磁电弹材料反平面切口奇性数值分析[J]. 中国科学: 物理学 力学 天文学, 2014, **44**(1): 91-99.(CHENG Changzheng, DING Hao, WANG Dapeng, et al. Numerical analysis of the singularities for a magneto-electroelastic notch under anti-plane deformation[J]. *Scientia Sinica: Physica, Mechanica & Astronomica*, 2014, **44**(1): 91-99.(in Chinese))

[34] YANG Y Y, CHENG C Z, YAO S L, et al. Singularity analysis for the V-notch in functionally graded piezoelectric/piezomagnetic material[J]. *Journal of Engineering Mathematics*, 2021, **132**(1): 17.

[35] CHEN C D, CHUE C H. Singular electro-mechanical fields near the apex of a piezoelectric bonded wedge under antiplane shear[J]. *International Journal of Solids and Structures*, 2003, **40**(23): 6513-6526.

[36] ALSHITS V I, DARINSKII A N, LOTHE J. On the existence of surface waves in half-infinite anisotropic elastic media with piezoelectric andpiezomagnetic properties[J]. *Wave Motion*, 1992, **16**(3): 265-283.

[37] NAN C W, CAI N, SHI Z, et al. Large magnetoelectric response in multiferroic polymer-based composites[J]. *Physical Review B: Condensed Matter and Materials Physics*, 2005, **71**: 014102.

[38] KUO H Y, SLINGER A, BHATTACHARYA K. Optimization of magnetoelectricity in piezoelectric-magnetostrictive bilayers[J]. *Smart Materials and Structures*, 2010, **19**(12): 125010.

[39] PATIL D R, CHAI Y, JEON B G, et al. Theoretical prediction of resonant and off-resonant magnetoelectric coupling in layered composites with anisotropic piezoelectric properties[J]. *Composite Structures*, 2017, **159**: 498-504.

[40] WANG H L, LIU B. The theoretical ultimate magnetoelectric coefficients of magnetoelectric composites by optimization design[J]. *Journal of Applied Physics*, 2014, **115**(11): 114904.

[41] LEUNG C M, ZHUANG X, XU J, et al. Importance of composite parameters in enhanced power conversion efficiency of Terfenol-D/PZT magnetoelectric gyrators[J]. *Applied Physics Letters*, 2017, **110**(11): 112904.

[42] CHUE C H, CHEN C D. Antiplane stress singularities in a bonded bimaterial piezoelectric wedge[J]. *Archive of Applied Mechanics*, 2003, **72**(9): 673-685.

[43] RAMIREZ F, HEYLIGER P R, PAN E. Free vibration response of two-dimensional magneto-electro-elastic laminated plates[J]. *Journal of Sound and Vibration*, 2006, **292**(3/4/5): 626-644.

[44] JIANG S N, JIANG Q, LI X F, et al. Piezoelectromagnetic waves in a ceramic plate between two ceramic half-spaces[J]. *International Journal of Solids and Structures*, 2006, **43**(18/19): 5799-5810.

[45] JARNG S S. Magnetostrictive Terfenol-D material linear simulation using finite element method[J]. *International Journal of Applied Electromagnetics and Mechanics*, 2006, **24**(3/4): 187-193.